Nano Research

ISSN 1998-0124 CN 11-5974/O4
https://doi.org/10.26599/NR.2026.94908433

Research Article

Polyhedral oligomeric silsesquioxane (POSS) constructed stable cross-linking network in polyimide for enhanced flame retardant, mechanical and corona resistance properties

Xian Cheng[1,§], Chenxi Wang[1,§](✉), Di Lan[2], Zihao Tang[1], Shuo Chen[1], Wenhao Zhang[1], Xinfeng Zhou[3], Leyuan Zhang[1], Guanglei Wu[4](✉)

[1] School of Electrical and Information Engineering, Zhengzhou University, Zhengzhou 450001, China

[2] School of Automotive Materials, Hubei University of Automotive Technology, Shiyan 442002, China

[3] Beijing Key Laboratory of Advanced Functional Polymer Composites, Beijing University of Chemical Technology, Beijing 100029, China

[4] College of Materials Science and Engineering, Qingdao University, Qingdao 266071, China

[§] Xian Cheng and Chenxi Wang contributed equally to this work.

Nano Res., **Just Accepted Manuscript** • https://doi.org/10.26599/NR.2026.94908433

https://www.sciopen.com/journal/1998-0124 on Jan. 12, 2026

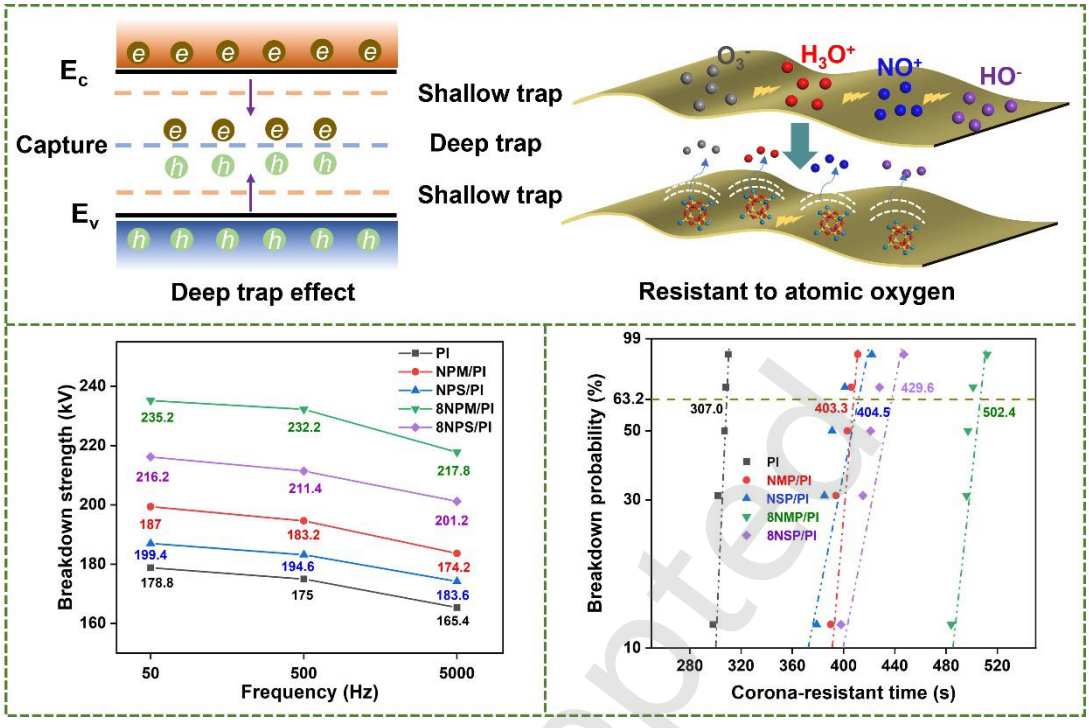

For the first time, diverse structural modifications of PI molecular chains were achieved by incorporating cage-like octa(aminopropyl) silsesquioxane was used to optimize and modify PI composites in this study. By doping the films with POSS, 8NMP/PI has shown significant improvements in thermal stability, mechanical strength, and corona resistance duration.

Nano Research

Open Access

Research Article

Polyhedral oligomeric silsesquioxane (POSS) constructed stable cross-linking network in polyimide for enhanced flame retardant, mechanical and corona resistance properties

Xian Cheng[1,§], Chenxi Wang[1,§] ✉, Di Lan[2], Zihao Tang[1], Shuo Chen[1], Wenhao Zhang[1], Xinfeng Zhou[3], Leyuan Zhang[1], and Guanglei Wu[4]✉

[1] *School of Electrical and Information Engineering, Zhengzhou University, Zhengzhou 450001, China*
[2] *School of Automotive Materials, Hubei University of Automotive Technology, Shiyan 442002, China*
[3] *Beijing Key Laboratory of Advanced Functional Polymer Composites, Beijing University of Chemical Technology, Beijing 100029, China*
[4] *College of Materials Science and Engineering, Qingdao University, Qingdao 266071, China*
[§] *Xian Cheng and Chenxi Wang contributed equally to this work.*

Received: 29 November 2025; **Revised:** 2 January 2026; **Accepted:** 12 January 2026

✉ Address correspondence to Chenxi Wang, chengxian@zzu.edu.cn; Guanglei Wu, wuguanglei@mail.xjtu.edu.cn, wuguanglei@qdu.edu.cn

Cite this article: *Nano Research*, **2026**, *19*, 94908433. https://doi.org/10.26599/NR.2026.94908433

ABSTRACT: As electrical equipment is progressively advancing towards high-power and large-capacity integration, the electrical insulation components frequently experience severe structural damage and performance degradation when they are exposed to significant voltage impact. Modifying the insulating base materials through filling to enhance their corona resistance is a critical measure to ensure the safe operation of electrical equipment. This article proposes, for the first time, a distinct modification strategy of cage-like octa(aminopropyl) silsesquioxane ($8NH_2$-POSS) particle toward the molecular structure of polyimide. This particle can form covalent bonds with both the main chains and side chains of polyimide (PI) during polymerization, thereby enhancing the flame retardant, mechanical and corona resistance of the polyimide matrix. Benefiting from the organic-inorganic hybrid structure, the POSS with amino groups provides interfacial compensation for PI at the molecular structural level. The power frequency breakdown strength of the $8NH_2$-POSS main-chain grafted PI composite film (8NMP/PI) is increased by 31.5%, and the corona discharge inception voltage is enhanced from 1.93 to 2.13 kV. And the average corona resistance time of 8NMP/PI is prolonged from 305 to 498 s, which is 63.3 % higher than the pure PI film. Meanwhile, its excellent interface effect improves the flexibility of the composite film, with the average tensile strength increased by 17.6% and the elongation at break by 16.2 %. All composite films have reached UL-94 V-0 rating. This work provides valuable reference for developing high-performance polymer composites for applications in large-scale electrical devices.

KEYWORDS: POSS, flame retardant, inorganic-organic hybrid, mechanical properties, corona resistant capacity

1 Introduction

With the advancement of modern industrial production and power electronic equipment, the service life of traditional insulating materials under complex working conditions fails to meet expectations [1-3]. Currently, intensive attention focuses on developing insulation composites that can adapt to complicated working environments. Consequently, mechanically flexible insulation polymer composites have become the objective of insulation barriers for large-scale equipment. [4, 5]. Polyimide has been extensively applied in various fields such as electronic devices, aerospace, and high-performance coatings owing to its outstanding insulation properties, thermal stability, mechanical strength, and chemical resistance [6-9]. Moreover, it plays a critical role in ensuring the insulation stability of motor windings. The intrinsic properties of polyimide can be enhanced through methods such as structural modification and nanocomposite filling. By introducing flexible groups or long molecular chains into the main or side chains during the polymerization process, its solubility, processability, or thermal stability can be improved [10, 11]. Yu et al [12] introduced the rigid (DAPBI-BTDA) and flexible (ODA-BTDA) monomer unit into PI molecular chains. By adjusting the ratio of rigid to flexible elements, they obtained PI films with a series of different structures, exhibiting excellent thermal stability and mechanical properties. Song et al [13] reported the effect on the solubility of composite films when 2,2'-dichloro substituted biphenyl linkage was introduced into polyimide mainchain. The results indicated that the modified PI could dissolve in a range of polar solvents, greatly enhancing its solubility properties. The structural modification of polyimide is primarily employed in studies on heat resistance and solubility properties. However, its large-scale application is limited by issues such as complex processing and high costs. When hybridized with inorganic nanoparticles, their unique properties can enhance impart the polymer matrix. For example, Al_2O_3, BN, and CNTs can enhance the insulation, optical, and conductive characteristics of the polymer, making it suitable for various applications [14-17]. Wang et al. [18] utilized a layered solution casting method to fabricate the Janus structured MXene/polyimide bilayer composite films. Its unique model of "conductive on one side and insulating on the other" achieved excellent shielding performance. Luo et al. [19] designed a multifunctional CNTs@$CoFe_2O_4$/polyimide aerogel, which achieved lightweight properties while delivering excellent thermal insulation and electromagnetic wave absorption performance. Ai et al. [9]

effectively improved the breakdown strength and charge-discharge efficiency of the polyimide matrix by incorporating two-dimensional Al_2O_3 nanoplates. As a result, the directional compensation of polyimide properties can be achieved by introducing different nanoparticles into the PI matrix.

In recent years, polyhedral oligomeric silsesquioxane (POSS) has garnered widespread attention due to its unique structural properties, enabling organic-inorganic nanohybridization at the molecular level. The silicon-oxygen cage structure of the POSS core possesses high thermal stability and atomic oxygen resistance. Furthermore, functional groups such as epoxy, amino, and phenyl groups on its periphery endow POSS nanoparticles with functionality and high reactivity [20-24]. This allows them to form various cross-linked network structures with other polymers, thereby imparting the polymer materials with excellent heat resistance and chemical resistance. Additionally, the porous structure of POSS improves the overall dielectric properties of the material [25-28]. Dong et al. [29] modified the molecular structure of polyimide with mono-amino POSS. The resulting composites exhibited excellent charge-discharge cyclability and discharge energy density. Qiao et al. [30] reported that the cubane-type POSS had achieved higher conductivity at room temperature. Qian et al. [31] used blends of trisilanolphenyl POSS to explore the atomic oxygen resistance of PI films, and the research verified that POSS cage structure could well resist the attack of atomic oxygen. Numerous studies have confirmed that the POSS structure can improve the electrochemical and antioxidant properties of polymers [32-34]. However, there are currently few reports on the impact of POSS on the electrical properties of polymers, and almost no research has been mentioned regarding the role of POSS in achieving corona resistance in polymers.

In this work, we employed molecular design strategies to incorporate POSS grafted with varying numbers of amino groups into the polyimide structure. By utilizing the amino groups to react with pyromellitic dianhydride, POSS was integrated into the polymer main chain. Subsequently, through esterification with the carboxyl groups on the side chains of the precursor polyamic acid, differently functionalized POSS/PI composite films were obtained. The research revealed the effects of POSS organic groups, introduced via different methods, on the dielectric and corona resistance properties of the composite films. Fig. 1 shows the reaction mechanism and flowchart for the preparation of 8NMP/PI, while Fig. S1 illustrates the synthetic reaction equation of 8NSP/PI. This research provides novel insights for the enhancement of polymer properties through various hybrid structures of POSS.

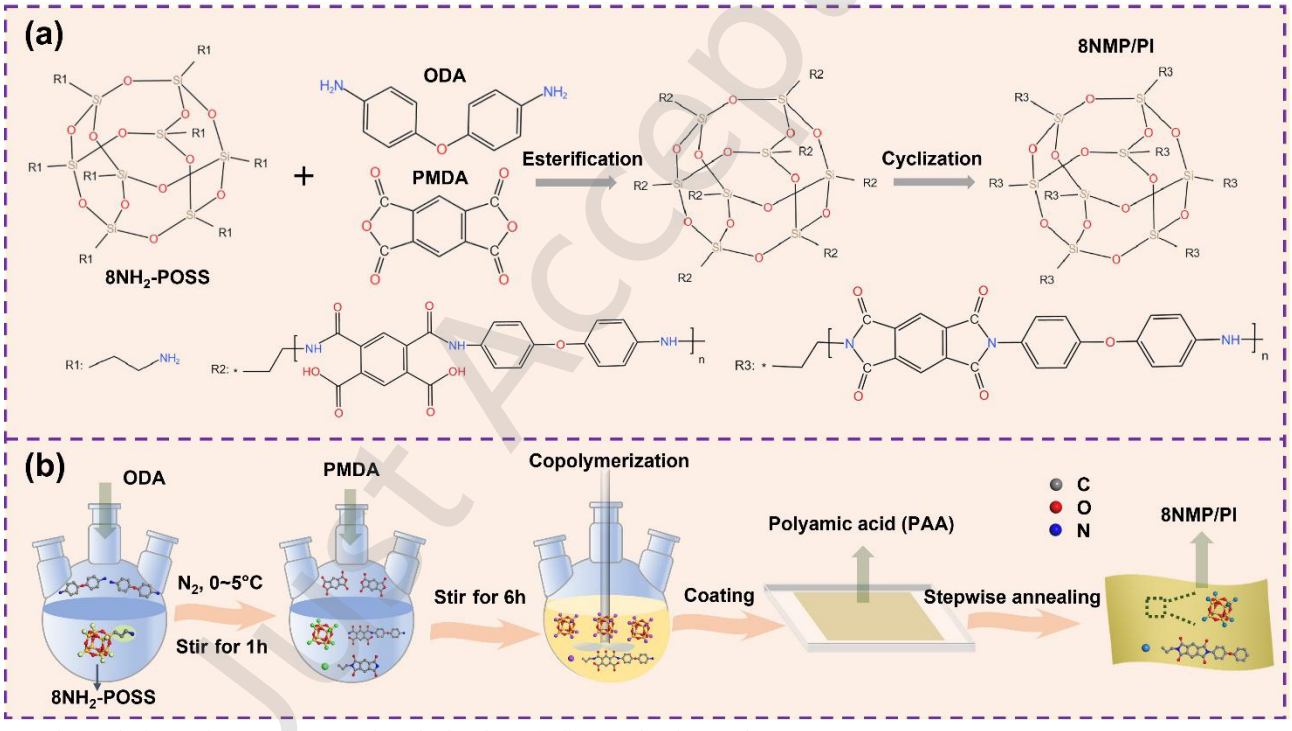

Figure 1 The synthetic reaction equation (a) and synthesis schematic diagram (b) of 8NMP/PI.

2 Experimental

2.1 Materials

Anhydrous N, N-Dimethylacetamide (DMAc, $CH_3CON(CH_3)_2$), Pyromellitic anhydride (PMDA, $C_{10}H_2O_6$), 4,4'-Oxydianiline (ODA, $C_{12}H_{12}N_2O$), Aminopropyllsobutyl POSS were purchased from Shanghai Macklin Biochemical Technology Co., Ltd., Octa(aminopropyl) silsesquioxane POSS were purchased from Xi'an Haoran Biological Technology Co., Ltd.

2.2 Synthesis of PI film.

2.002 g of ODA was first dissolved in a three-neck flask with 40.4 mL of anhydrous DMAc. Then, 2.224g of PMDA were added in three times, each addition was spaced one hour apart. The polyamic acid solution was obtained by stirring above solution for 6 hours until the reaction complete. The experiment process was conducted under a nitrogen protection system, with the reaction temperature maintained between 0 and 5℃. After removing the internal bubbles from the polyamic acid under vacuum, the solution was poured onto a clean glass plate. A coater was adjusted to spread the film evenly, the PI film was obtained after thermal imidization at 80, 160, 220, and 280 °C, holding for 1 h at each temperature stage. The thickness of final film was approximately 25 μm.

2.3 Synthesis of 8NH_2-POSS/PI (NH_2-POSS/PI) films with different grafting methods.

First, 55.1 mg of 8NH_2-POSS (NH_2-POSS) was added to a three-neck flask containing 40.4 mL of anhydrous DMAc, and ultrasound stirring for 1 hour. Then, add 2.002 g of ODA and stir for another hour until completely dissolved. Subsequently, 2.224 g of PMDA were added in three times, each addition was spaced one hour apart. Follow the subsequent steps consistent with the procedure for pure PI film to obtain the main-chain-incorporated 8NH_2-POSS/PI (NH_2-POSS/PI), and the composites were named 8NMP/PI (NMP/PI). Add an equivalent amount of 8NH_2-POSS (NH_2-POSS) to the prepared polyamic acid, mix thoroughly, and then proceed with film formation and curing to obtain the side-chain-incorporated 8NH_2-POSS/PI (NH_2-POSS/PI) which named 8NSP/PI (NSP/PI).

2.4 Materials characterizations

The microstructure and morphology as-prepared samples were characterized by Field emission scanning electron microscopy (F-SEM; JEOL JSM-7800F). The surface functional groups of the samples were studied by Fourier transform infrared spectroscopy (FT-IR, Nicolet iS50). The crystalline structure of sample was described by the powder X-ray diffraction (XRD, Rigaku Ultima IV with Cu-Ka radiation, λ=1.5406 nm) in the range of 3-90° and X-ray photoelectron spectroscopy (XPS; AXIS Supra). The thermogravimetric curve was measured by the thermogravimetric analyzer (TGA, HTG/HQG-1). Differential Scanning Calorimetry (DSC) curves were measured by Differential Scanning Calorimetry Analyser (DSC250), (Temperature range: 30-400 ℃); The tensile strength and elongation at break were evaluated using an electronic universal testing machine (34TM-30, Instron, USA) at a crosshead speed of 10 mm/min; The dielectric constant and loss tangent were obtained and calculated by Impedance analyzer (E4990A); The breakdown field strength and corona resistance voltage of the material at different frequencies were measured by an aging test platform built in the laboratory, as shown in Fig. S2. The electrode is spherical-plate which the diameter and thickness of plate is 20 mm and 5 mm, the diameter of the ball is 20 mm. The thickness of the film is 25 μm, and a square film of 25 mm × 25 mm is taken as the test sample. Before the corona test, the electrode needs to be ground with 400 mesh sandpaper, and the arithmetic average of the 5 test results is taken as the final result for both the breakdown voltage and the corona resistance time. Flame retardant rating was evaluated by using a CZF2/3 (Ning Bo, China), and strip films measuring 125 ×13 × 0.025 mm^3 underwent five parallel tests to meet the standard ASTM D3801-19.

3 Results and discussion

3.1 Properties analysis of composites

The XRD patterns are shown in Fig. 2, the amorphous peaks of all samples at 20-25° can be seen in Fig. 2(a), confirming the amorphous morphology of polyimide in the composites. In Fig. S3(a), NH_2-POSS exhibits the obvious diffraction peaks at 6.4° and 11.1°, which are attributed to the molecular chain backbone spacing. It can be seen from the Bragg's law ($2d\ sin\theta=n\lambda$) that 6.4° and 11.1° diffraction peaks corresponding to d-spacings of 13.8 and 8.0 A° is caused by the size of the NH_2-POSS molecules [35]. The wide peaks around 21.4° could be attributed to the molecular structure of the POSS cage. In Fig. S3(b), the crystalline characteristics of 8NH_2-POSS are more pronounced, with diffraction peaks in the range of 8-30° consistent with those reported in the literature [36]. NMP/PI and 8NMP/PI exhibit virtually no distinct diffraction peaks, attributed to the disruption of crystalline structures in composites where the POSS is homogeneously dispersed within the amorphous polyimide. The small-angle diffraction peaks observed in the range of 6-9° for NSP/PI and 8NSP/PI likely originate from aggregation caused by the inability of grafted POSS side chains to achieve uniform dispersion under high viscosity conditions. Fig. 2(b) is the FT-IR spectrum of samples, the C=O bending could be confirmed in polyimide by the absorption peak at 720 cm^{-1}. The peaks at 1712 and 1776 cm^{-1} represent the C=O of symmetrical stretching vibration and asymmetrical stretching vibration [37]. The appearance of the peak at 1366 cm^{-1} (C–N stretching), along with the disappearance of peaks at 1540 and 1645 cm^{-1} (characteristic of amide bands), indicates the successful conversion of the polyimide precursor via dehydration and cyclization [38]. The results showed that the imidization was almost complete, and the composites was successfully prepared in this work.

Fig. S4 show the full XPS spectra of all the samples, the binding energies of five films at 532, 400, 285, 154, and 102 eV represent the O 1s, N 1s, C 1s, Si 2s, Si 2p orbitals, respectively. The weak Si signal present in PI may be due to contamination of the glass plate onto the sample surface during sample preparation. Fig. 3(a) is five C1s fine spectra, and the three peaks nearby 284.6, 285.4 and 288.4 eV represent C−C, C−N, and N−C=O bonds [39-41]. However, the samples of NMP/PI, NSP/PI, 8NMP/PI and 8NSP/PI were confirmed the presence of C-Si by 284.2 eV peak. The peak of 400.2 eV in N1s (Fig. 3(b)) can be attributed to the C−N bond of the amide in PI [19]. The high-resolution O 1s spectra (Fig. 3(c)) can be deconvoluted into two or three peaks. The peaks around 532.1 and 533.4 eV are assigned to C–O and C=O bonds, respectively, while the peak at 534 eV can be attributed to the Si–O–Si bond formed after the introduction of POSS into the polyimide matrix [42]. Si 2p fine spectrums (3d) of NMP/PI, NSP/PI, 8NMP/PI and 8NSP/PI could be deconvoluted into two energy levels, respectively, the binding energies around 102 and 103 eV indicate the presence of Si−C and the Si−O bonds [43, 44].

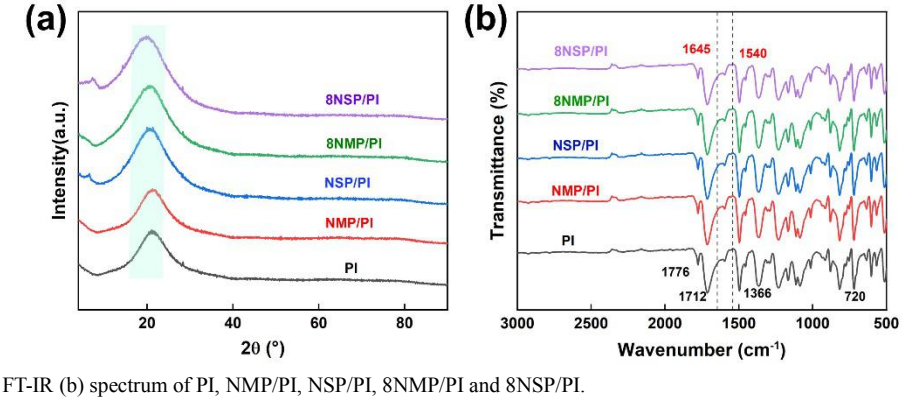

Figure 2 The XRD (a) and FT-IR (b) spectrum of PI, NMP/PI, NSP/PI, 8NMP/PI and 8NSP/PI.

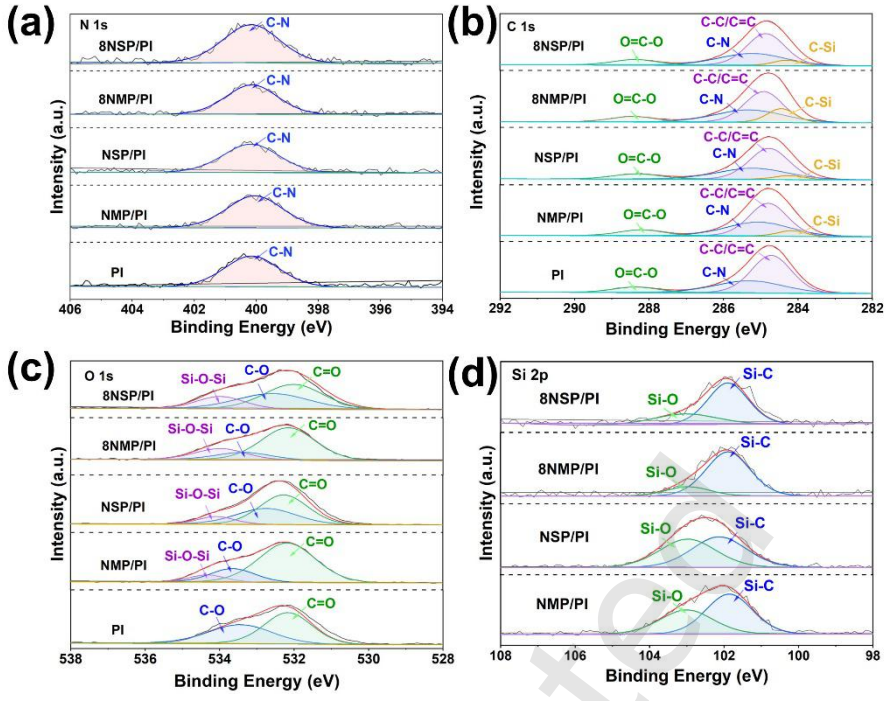

Figure 3 XPS spectrum of five samples: Fine spectrum: C 1s (a), N 1s (b), O 1s (c), Si 2p (d).

3.2. Thermal analysis of composites

Figs. 4(a) and 4(b) show the TGA and DSC curves of the samples, respectively. The TGA curves of all samples indicate that the polyimide begins to decompose around 500°C. At 5% weight loss, the decomposition temperature ($T_{5\%}$) of pure PI is 496.3°C, while those of NMP/PI, NSP/PI, and 8NMP/PI are approximately 508°C. It is worth noting that decomposition temperature of 8NSP/PI film has reached 515.1°C, achieving an enhancement of 18.8 °C compared to the pristine PI film. The DSC curve in Fig. 4(b) shows that the pure PI exhibits a glass transition temperature (T_g) of 372.2°C, which is consistent with the reported T_g values of polypyromellitimide in the literature [11]. The thermal analysis results of PI and its POSS composites films are shown in Table 1. After introducing POSS, the T_g of all the composites increased, with the side-chain grafted PI demonstrating more significant enhancement. This improvement could be attributed the steric hindrance effect of the bulky side-chain molecules, which restricts the movement of the PI main chains, thereby elevating the glass transition temperature [45, 46]. The results show that the POSS not only does not destroy the intrinsic thermal properties of polyimide, but even increases its pyrolysis and glass transition temperature.

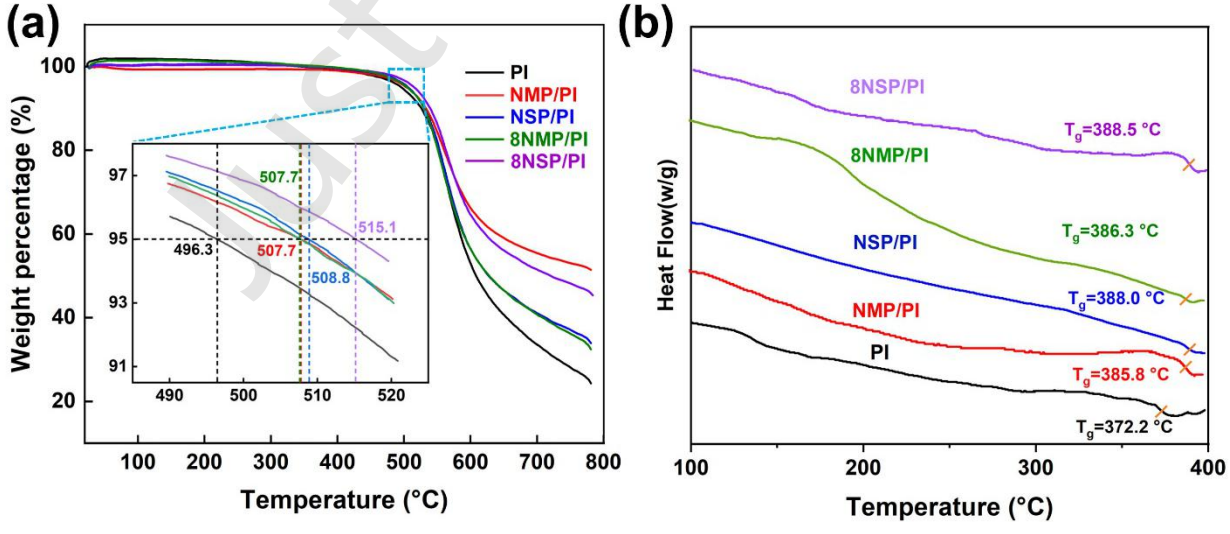

Figure 4 (a) and (b) are the TG and DSC curves of PI, NMP/PI, NSP/PI, 8NMP/PI and 8NSP/PI.

Table 1. Thermal analysis results of pure PI and POSS/PI composites films.

Samples	$T_{5\%}$ (℃)	T_g (℃)	$T_{5\%}$ increase (℃)	T_g increase (℃)
PI	496.3	372.2	\	\
NMP/PI	507.7	385.8	11.4	13.6
NSP/PI	508.8	388.0	12.5	15.8
8NMP/PI	507.7	386.3	11.4	14.1

8NSP/PI	515.1	388.5	18.8	16.3

Both pure polyimide and composite films were subjected to the UL-94 vertical burning test. Figs. 5 and S5 demonstrate the combustion state of the films at different time intervals. The samples exhibited low smoke emission and almost no melting drips during combustion. Particularly for the POSS-modified films, they immediately self-extinguished after flame removal, achieving a UL-94 V-0 rating. The excellent flame-retardant properties could be attributed to the protective char layer formed from pyrolyzed PI molecular chains (Fig. 6), while the dense SiO_2 layer generated by POSS under high temperatures further inhibited flame propagation [47-49].

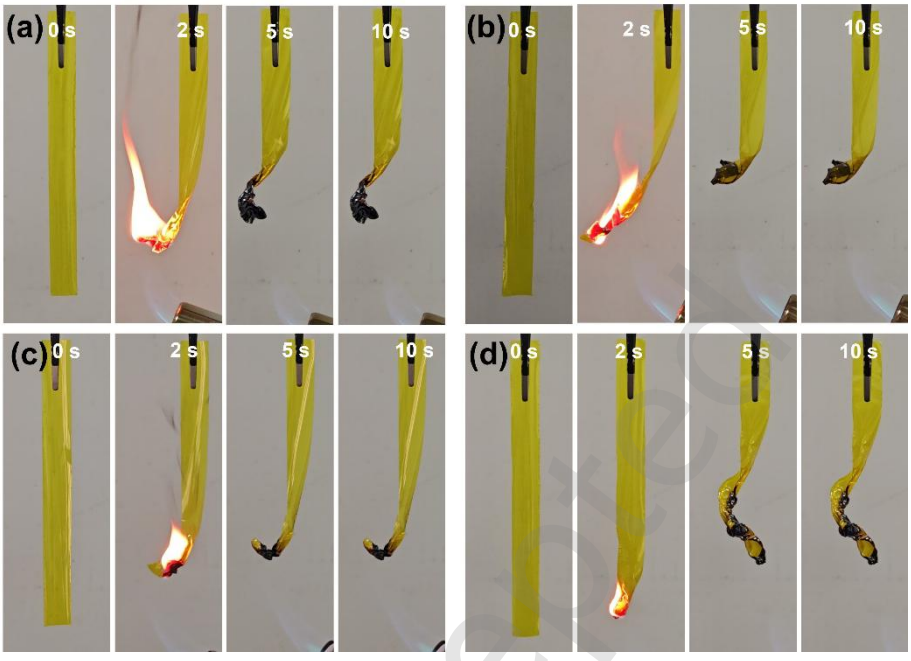

Figure 5 UL-94 digital images of NMP/PI (a), NSP/PI (b), 8NMP/PI (c) and 8NSP/PI (d).

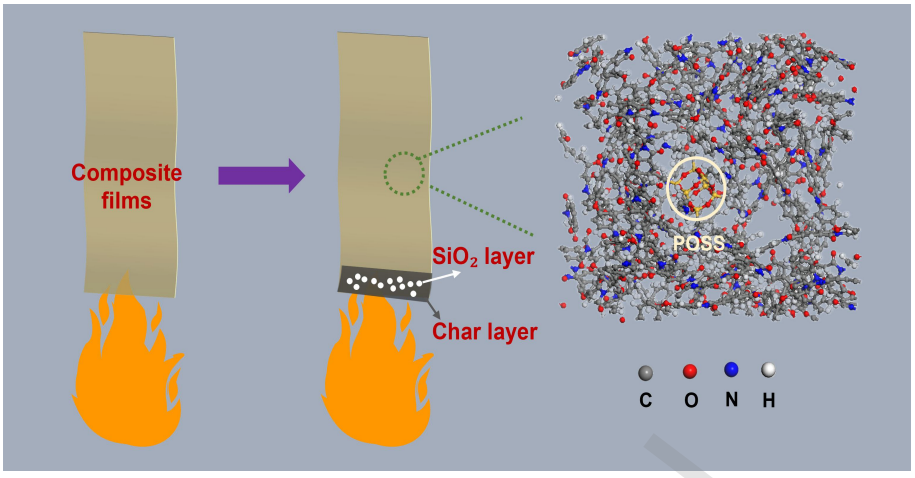

Figure 6 Flame retardant mechanism of the composite films.

3.3 Mechanical analysis

Figs. 7(a1-a5) are the optical images of the PI, NMP/PI, NSP/PI, 8NMP/PI and 8NSP/PI films, it can be seen that the surface of PI and other composites are smooth and exhibit good light transmittance. Figs. 7(b1-b5) are SEM images of PI, NMP/PI, NSP/PI, 8NMP/PI and 8NSP/PI, respectively, and the surface of the pure PI film is smooth and flat, without obvious impurities. It can be seen from Figs. S6(a) and (b) that NH_2-POSS and 8NH_2-POSS have two-dimensional sheet structure, with sizes ranging from nanometers to micrometers. The lamellar particles of the POSS main chain linked NMP/PI and 8NMP/PI in Figs. 7(b2) and 7(b4) are evenly dispersed, due to the sonication before synthesis. The POSS distribution in Figs. 7(b3) and 7(b5) tends to be stacked, which is due to the viscosity of the polyimide precursor leading to the POSS in the subsequent process unable to disperse completely during the reaction. The SEM and energy dispersive spectroscopy (EDS) mapping images of the 8NMP/PI and 8NSP/PI in Figs. S7 (a, b) show that the elements such as C, O, and N are distributed homogeneously, the Si element is concentrated in the region of particle hybridization. Fig. 7(c) displays the stress-strain curves of all samples. The PI film demonstrates a tensile strength of 88.1 MPa (Fig. 7(d)) and elongation at break of 22.2% (Fig. 7(e)). However, both NMP/PI and 8NSP/PI hybrid materials exhibit inferior mechanical properties compared to the pure film. This phenomenon can be explained that the mono-amino groups in NH_2-POSS tend to terminate the molecular chains of polyimide when incorporated into the main chain structure, preventing the formation of long polymer chains for NMP/PI. This chain termination effect ultimately reduces composites both tensile strength and fracture elongation relative to the PI film. For 8NSP/PI, the decreased breaking elongation (down to18.9%) may result from two concurrent mechanisms. On the one hand, the agglomeration effect caused by POSS particles during side chain incorporation. On the other hand, the restricted material flexibility due to lateral cross-linked structures formed between multiple terminal active groups on POSS and PI molecular chains [50-52]. In NSP/PI composites, although NH_2-POSS exhibits some aggregation, the its smaller size structure forms an interface with PI could reduce cracks between molecular chains [53]. Additionally, the mono-amino groups preserve the integrity of the polymer molecular chain structure, resulting in the maintenance of the elongation at break. The excellent dispersion of 8NH_2-POSS and its favorable interfacial compatibility with PI play a vital role in improving the tensile strength of 8NMP/PI. The chemical grafting of active groups on the cage-like POSS to the main chains of polyimide molecules enhances the composites' stability. When the material is subjected to mechanical stress, the external load can be effectively transferred to the rigid POSS cages via these chemical bonds, which enhances the tensile strength of the material [54]. Furthermore, the improvement in elongation at break can be attributed to the introduction of hollow cage-like POSS structures, which increase the free volume within the composite films. This phenomenon impedes the tight stacking of PI molecular chains, allowing for local chain rotation before fracture, thereby improving the elongation at break of the polyimide. Consequently, the 8NMP/PI hybrid film achieves the average tensile strength of 103.6 MPa and a breaking elongation of 25.8 %, being improvements of 17.7% and 16.2 %, respectively, compared to pure PI.

3.4 Electrical analysis

The dielectric parameters can effectively reflect its charge storage and polarization capacity [55]. Figs. 8a and 8b illustrate the dielectric and dielectric losses of the composites at different frequencies, respectively. The decrease in dielectric constant with increasing frequency can be attributed to the relaxation phenomenon of various polarization effects within the sample, especially dipole polarization. The dipole polarization could not respond to the alternating electric field at high frequencies [56, 57], leading to a decrease in overall polarization. The dielectric constant of pure PI is within the range of 3.08-3.16. The overall dielectric constant of all hybrid materials decreases, primarily due to the increased free volume in the composites and the intrinsic porosity introduced by POSS [58]. For 8NH_2-POSS, its large surface dimensions could introduce more free volume in composites. Furthermore, the eight amino groups on POSS react with the carboxyl groups (polar functional groups) on the polymer molecular chains to form peptide bonds, thereby reducing the polarity of the hybrid material. As a result, the dielectric constant of 8NMP/PI decreases to 2.87-2.94. In the case of 8NSP/PI hybrid materials, the side-chain grafting may introduce additional free volume, leading to a further reduction in the dielectric constant to 2.70-2.76. Compared to pure PI films, 8NMP/PI and 8NSP/PI have a lower dielectric loss. The dielectric loss of NMP/PI and NSP/PI is almost the same as that of the pure film at low frequencies, while at high frequencies, the dielectric loss begins to decrease. It indicates that the incorporation of POSS reduces dielectric loss at high frequencies by weakening the composites' dielectric response. Fig. 8(c) shows the average breakdown field strength of composite films at power frequency 50, 500 and 5000 Hz. It can be seen from polyline variation, the breakdown field strength decreases with increasing frequency, indicating that higher frequency electric fields cause more severe damage to insulating materials. The PI film exhibits a breakdown field strength of 178.8 kV/mm at power

frequency, then decreases to 165.4 kV/mm at 5000 Hz which have a 7.5% reduction compared to the power frequency.

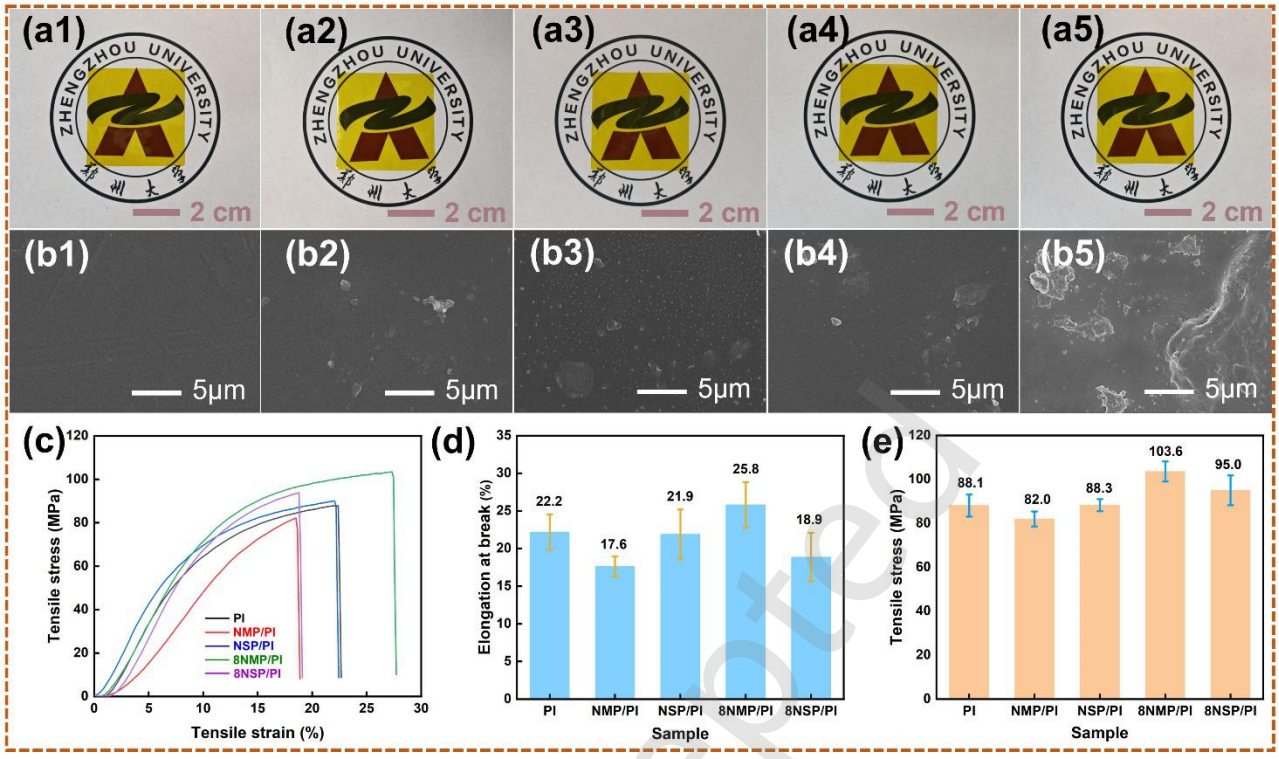

Figure 7 The digital images of PI (a1), NMP/PI (a2), NSP/PI (a3), 8NMP/PI (a4) and 8NSP/PI (a5); The SEM images of PI (b1), NMP/PI (b2), NSP/PI (b3), 8NMP/PI (b4) and 8NSP/PI (b5); The stress-strain curve (c) of PI, NMP/PI, NSP/PI, 8NMP/PI and 8NSP/PI composites; The average tensile strength (d) and breaking elongation (e) of PI, NMP/PI, NSP/PI, 8NMP/PI and 8NSP/PI composites.

All POSS/PI hybrid materials show enhanced breakdown strength (Fig. S8 includes error bars). The breakdown field strength of 8NMP/PI has reached 235.2 kV/mm at power frequency, marking a 31.5% improvement over the PI film. 8NMP/PI also maintains a breakdown field strength of 217.8 kV/mm at 5000 Hz, corresponding to a 31.7% enhancement compared to the pure film. These results indicate that frequency would not significantly impact the breakdown field strength improvement of the composite materials. The breakdown voltages of different samples are analyzed using the two-parameter Weibull distribution algorithm. The expression for the cumulative failure probability of breakdown is given as [9]

$$P(E) = 1 - e^{-\left(\frac{E}{E_b}\right)^{\beta}}$$

Where *P(E)* is the cumulative breakdown probability, *E* and E_b are the actual breakdown field and characteristic Weibull breakdown strength (63.2% failure probability), respectively. β is the shape parameter which reflects the scatter of breakdown voltage. Figs. 8(d-f) illustrate the Weibull distribution curves under power frequency 50, 500 and 5000 Hz, respectively. The electric fields corresponding to a 63.2% breakdown failure probability for PI, NMP/PI, NSP/PI, 8NMP/PI, and 8NSP/PI are 182.2, 190.1, 202.9, 239.9, and 220.1 kV/mm at 50 Hz, respectively. The modified PI exhibited a maximum enhancement of 57.7 kV/mm compared to pure PI. Under the three frequencies, the breakdown field strengths of the composites at the 63.2% breakdown failure probability are all improved compared to pure PI, especially 8NMP/PI and 8NSP/PI. The low dielectric constant indicated that there was less polarization in the materials, and the cross-linked network structure effectively restricted carrier migration [59, 60], thereby significantly improving the breakdown field strength of the composite films.

The discharge phenomenon of 8NSP/PI was observed by optical images in Fig. 9(a) at 2.5 kV-5kHz voltage and frequency (Fig. S9 is voltage waveform), and it exhibited uniform discharge arc. Fig. 9(b) shows the image of the sample breakdown after accelerated aging in Fig. 9(a). It can be seen that the central area of the contact electrode is burned out a small hole (Fig. S10 is the optical micrograph of the central breakdown region of the 8NMP/PI film). Fig. 9(c) illustrates the electrical breakdown process of the polymer molecular chains. The number of broken C–N and –C–O–C– bonds within chain segments increases with the extension of aging time under high-frequency and high-voltage conditions. Fig. 9(d) shows the partial discharge inception voltages (corona inception voltages) of the five films. The average discharge inception voltage of the pure film is 1.93 kV, while that of 8NMP/PI is 2.13 kV which has a 10.4% increase compared with the pure film. Fig. 9(e) displays the Weibull distribution of the discharge inception probability for the films, the voltages corresponding to a 63.2% discharge probability for PI, NMP/PI, NSP/PI, 8NMP/PI, and 8NSP/PI are 1.96, 2.05, 2.01, 2.16, and 2.07 kV, respectively. These results confirm that the POSS cage structure mitigates electric field distortion by homogenizing charge distribution to effectively suppress discharge in the composite materials [61]. The corona resistance time of different films under accelerated aging conditions at 2.5 kV-5 kHz voltage and frequency was obtained by Fig. 9(f). The average corona resistance lifetime of 8NMP/PI reached 498 s, which is an increase of 63.3%, 24.3%, 25.9%, and 18.1% compared to pure PI (305 s), NMP/PI (400.8 s), NSP/PI (395.6 s), and 8NSP/PI (421.8 s), respectively. Notably, the corona resistance time corresponding to a general failure probability (63.2%) in Weibull distribution is closely correlated with the average corona resistance time of all samples (Fig. 9(g)).

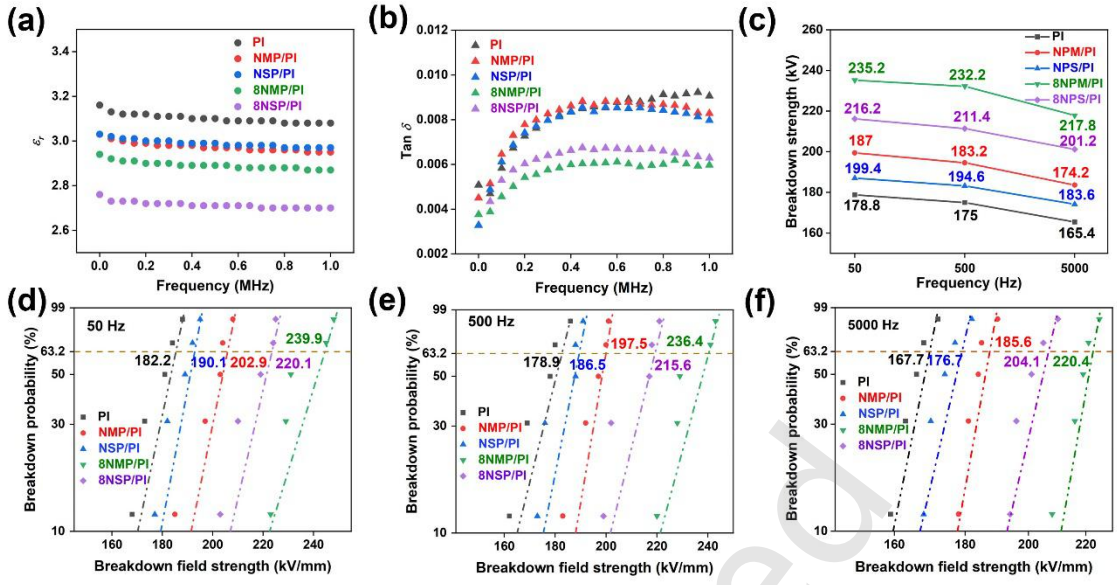

Figure 8 The dielectric constant (a) and dielectric loss (b) of PI, NMP/PI, NSP/PI, 8NMP/PI and 8NSP/PI; (c) is the average breakdown field strength of PI, NMP/PI, NSP/PI, 8NMP/PI and 8NSP/PI at 50, 500 and 5000 Hz; The Weibull distribution of PI, NMP/PI, NSP/PI, 8NMP/PI and 8NSP/PI at 50 (d), 500 (e) and 5000 Hz (f).

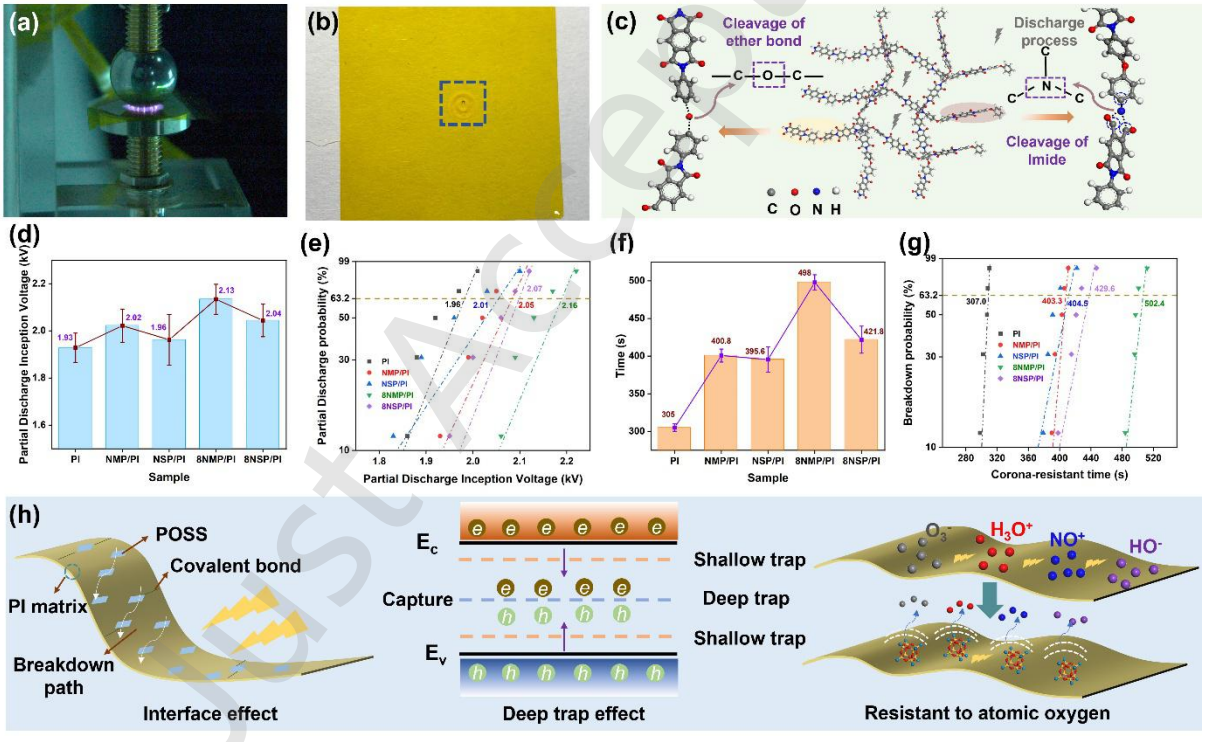

Figure 9 The discharge arc (a) and (b) breakdown digital images of 8NSP/PI; (c) represents the electrical aging-induced degradation process of the polymer;(d) and (e) are the average partial discharge inception voltages and its Weibull distribution patterns of PI, NMP/PI, NSP/PI, 8NMP/PI and 8NSP/PI; (f) and (g) are the average corona resistance time and its Weibull distribution of PI, NMP/PI, NSP/PI, 8NMP/PI and 8NSP/PI (h).

As shown in Fig. 9(h), the enhanced corona resistance of POSS-modified composites can be attributed to its cage-like organic-inorganic structure and interfacial reinforcement effect (via chemical bonding) with organic matrices, which passivates internal micro-defects. Particularly in the 8NMP/PI composites, uniformly dispersed $8NH_2$-POSS particles effectively obstruct the corona-induced damage propagation path and prolong the voltage breakdown pathway. As high-energy electrons propagate through the material, the scattering occurs on collisions with POSS particles. This process attenuates the electrons' energy, which further suppresses the formation and development of electron avalanches. Moreover, the introduced POSS particles may create abundant deep traps capable of capturing high-energy electrons and reduce space charge accumulation within the material may be a critical reason to improve the corona resistance of the composites. Meanwhile, the substantial amounts of ions such as O_3^-, HO^-, H_3O^+, and NO^+ will be generated on the polyimide surface during corona discharge processes [62, 63]. Notably, the SiO_2 structure within POSS can exhibit outstanding resistance to atomic oxygen, effectively inhibiting surface oxidation of the film during corona discharge. The evident improvement in the material's corona resistance time is primarily attributed to the synergistic mechanism between the erosion resistance of the inorganic skeleton and the modulation of deep trap energy levels. In short, POSS modified polyimide could be an excellent candidate for a high electrical performance material.

4 Conclusions

In summary, polyhedral oligomeric silsesquioxane cross-linking network in polyimide was constructed by different grafting methods. The 8NMP/PI exhibited stable thermodynamics and outstanding mechanical properties with a high tensile strength (103.6 MPa) and an enhanced breaking elongation, which improved 17.6 % and 16.2 % than PI film, respectively. All POSS/PI hybrid materials demonstrate lower dielectric properties, higher breakdown strength, and superior corona resistance characteristics, which are attributed to the unique cage-like structure and intrinsic properties of POSS. Specifically, the 8NMP/PI composites exhibit breakdown strength improvements of 31.5, 32.7, and 31.7% compared to pure PI at 50, 500 and 5000 Hz, respectively. Under accelerated aging conditions at 2.5 kV-5000 Hz, 8NMP/PI average corona resistance time reached 498 s, being more than PI by 63.3 %. These results demonstrate that using the distinctive cage-like architecture of POSS and organic-inorganic hybrid characteristics to modify polymer matrix has emerged as an innovative strategy for significantly enhancing both mechanical and electrical performance.

Electronic Supplementary Material: Supplementary material (mechanism reaction of samples and the test systems for breakdown and corona resistance of films. Additional experimental details including the POSS fillers and the composites' digital images, SEM images, XRD and XPS spectra, aging voltage waveform, breakdown field strength)

Data availability

All data needed to support the conclusions in the paper are presented in the manuscript and the Electronic Supplementary Material. Additional data related to this paper may be requested from the corresponding author upon request.

Acknowledgments

This work was supported in part by the National Special Support Program for High-Level Talents (Project No. SQ2022QB06966), and by the National Nature Science Foundations of China (Project No. 52477162 and No. 52477163), and by the Key Research and Development Program of Henan Province (Project No.251111241200), by Henan Province Zhongyuan Electric Laboratory (Project No. zd20250402), by Henan Province University Science and Technology Innovation Team Support Program (25IRTSTHN012), by Henan Province Science and Technology Research Project Program (242102241060), and by Henan Province Reform and Quality Enhancement of Postgraduate Education（YJS2025XQLH08).

Declaration of competing interest

All the contributing authors report no conflict of interests in this work.

Author contribution statement

X. C.: Data curation, funding acquisition, validation, writing manuscript, experimental design. C. X. W.: Data curation, validation, writing manuscript, experimental design. Z. H. T.: Data curation, writing manuscript. S. C.: Data curation. W. H Z.: Data curation. X. F. Z.: validation. L. Y. Z.: validation. D. L.: validation. G. L. W.: Funding acquisition, writing manuscript, experimental design.

Use of AI statemen

None.

References

[1] Yuan, H. W.; Wang, Z.; Lan, D.; Zhang, S. Y.; Zang, Z. C.; Jiang, G. Q.; Wei, H. C.; Zhang, Y. Y.; Zheng, J. J.; Ren, J. W.; Wu, G. L.; Jia, S. L. Aramid nanofibers at ultralow loadings: driving significant multifunctionality in epoxy composite dielectrics. *Adv. Compos. Hybrid. Mater.* **2025**, *8*, 161.

[2] Tang, L.; Ruan, K. P.; Liu, X.; Tang, Y. S.; Zhang, Y. L.; Gu, J. W. Flexible and robust functionalized boron Nitride/Poly(p- Phenylene Benzobisoxazole) nanocomposite paper with high thermal conductivity and outstanding electrical insulation. *Nano-Micro Lett.* **2024**, *16*, 38.

[3] Adnan, M. M.; Tveten, E. G.; Glaum, J.; Ese, M. G.; Hvidsten, S.; Glomm, W.; Einarsrud, M. Epoxy-based nanocomposites for high-voltage insulation: a review. *Adv. Electron. Mater.* **2019**, *5*, 1800505–1800527.

[4] Jia, M. S.; Tang, L.; Lin, Y. H.; Zeng, X. X.; Ruan, K. P.; Li, M. K.; Guo, Y. Q.; He, M. K.; Tang, Y. S.; Gu, J. W. Interfacial engineering for improving thermal conductivities of BNNS/PNF nanocomposite paper with superior electrical insulation and mechanical properties. *J. Mater. Sci. Technol.* **2026**, *254*, 126–134.

[5] Chen, Q.; Huo, S. Q.; Lu, Y. X.; Ding, M. M.; Feng, J. B.; Huang, G. B.; Xu, H.; Sun, Z. Q.; Wang, Z. Z.; Song, P. G. Heterostructured Graphene@Silica@Iron phenylphosphinate for fire-retardant, strong, thermally conductive yet electrically insulated epoxy nanocomposites. *Small* **2024**, *20*, 2310724.

[6] Wan, B. Q.; Zheng, M. H.; Yang, X.; Dong, X. D.; Li, Y. C.; Mai, Y. W.; Chen, G.; Zha, J. W. Recyclability and Self-Healing of Dynamic Cross-Linked Polyimide with Mechanical/Electrical Damage. *Energy Environ. Mater.* **2023** *6* 2575–0348.

[7] Ruan, K. P.; Li, M. K.; Pang, Y. H.; He, M. H.; Guo, H.; Shi, X. T.; Gu, J. W. Molecular Brush-Grafted Liquid Crystalline Hetero-Structured Fillers for Boosting Thermal Conductivity of Polyimide Composite Films. *Adv. Funct. Mater.* **2025**, *35*, 2506563.

[8] Ma, J. M.; Liu, X. F.; Wang, R. W.; Lu, C. X.; Wen, X. Q.; Tu, G. L. Research progress and application of polyimide-based nanocomposites. *Nanomaterials* **2023**, *13*, 656.

[9] Ai, D.; Han, Y. T.; Xie, Z. L.; Pang, X.; Chang, Y.; Li, H.; Wu, C. L.; Cheng, Y. G.; Wu, G. L. High temperature polyimide nanocomposites containing two-dimensional nanofillers for improved thermal stability and capacitive energy storage performance. *Nano Res.* **2024**, *17*, 7746–7755.

[10] Kong, Q. Q.; Zhang, J. L.; Zhang, K. Wang, S. S.; He M. K.; Guo, Y. Q.; Gu, J. W. Recyclable Side-Chain Azobenzene-Based Semicrystalline Polymer Films with Outstanding Intrinsic Thermal Conductivity and

Photoresponsive Actuation. *Angew. Chem. Int. Edit.* **2025**, *64*, e202512721.
[11] Li, S. E.; Zhu, H. R.; Bao, F.; Lan, X. Q.; Li, H.; Li, Y. D.; Ji, M. W.; Wang, M. L.; Zhu, C. Z.; Jian, X. Polyimide resins with superior thermal stability, dielectric properties, and solubility obtained by introducing trifluoromethyl and diphenylpyridine with different bulk pendant groups. *Polymer* **2023**, *283*, 126245.
[12] Yu, X. H.; Liang, W. H.; Cao, J. H.; Wu, D. Y. Mixed rigid and flexible component design for high-performance polyimide films. *Polymers* **2017**, *9*, 451.
[13] Song, G. L.; Chen, C.; Wang, X. Y.; Yao, J. N. Synthesis and properties of polyimides derived from 2,2'-dichloro-4,4',5,5'-biphenyltetracarboxylic dianhydride. *Polymer* **2019**, *183*, 121862.
[14] Luo, X. X.; Xie, H.; Ma, Y.; Lan, D.; Wu, G. L.; Jia, Z. R. Advances in iron-based electromagnetic wave absorbers: multiscale engineering from atomic defects to macroscopic architectures for performance optimization. *Int. J. Miner. Metall. Mater.* **2025**, doi: 10.1007/s12613-025-3252-1.
[15] Hao, Jiang.; Xie, Y. H.; He, M. K.; Li, J. D.; Wu, F.; Guo, Hua.; Guo, Y. Q.; Xie, D. L.; Mei, Yi.; Gu, J. W. Highly Thermally Conductive and Flame-Retardant Waterborne Polyurethane Composites with 3D BNNS Bridging Structures via Magnetic Field Assistance. *Nano-Micro Lett.* **2025**, *17*, 138.
[16] Morimune-Moriya, S.; Iwahashi, Y.; Nakamura, M.; Daisuke, O.; Nakamura, K. J. Covalent Introduction of Plasma-Treated carbon nanotubes into polyimide nanocomposites at Ultra-Low content. *Eur. Polym. J.* **2024**, *202***,** 112609.
[17] Jiang, W. H.; Xu, S.; Lv, C. P.; Lan, D.; Zhang, S. Y.; Gao, Z. G; Jia, Z. R.; Wu, G. L. Multi-scale Engineering of N-doped Carbon Nanofibers with Co3O4/CeO2 Heterostructures: Tailoring Heterointerface Polarization for Microwave Absorption. *Carbon* **2025**, *245*, 120784.
[18] Wang, L.; Yang, Z. L.; Lang, L.; Men, J. Y.; Gao, T. T.; Wang, Q.; Cheng, J. W.; Liu, Y. Z.; Zheng, N.; Liu, J.; Ji, X. H. Flexible multifunctional MXene/polyimide films with Janus structure for superior electromagnetic interference shielding. *Adv. Compos. Hybrid. Mater.* **2025**, *8*, 26.
[19] Luo, J. W.; Wang, Y.; Qu, Z. G.; Wang, W.; Yu, D. Anisotropic, multifunctional and lightweight CNTs@$CoFe_2O_4$/polyimide aerogels for high efficient electromagnetic wave absorption and thermal insulation. *Chem. Eng. J.* **2022**, *442*, 136388.
[20] Shi, M. G.; Ao, Y. Y.; Yu, L.; Sheng, L.; Li, S. X.; Peng, J.; Chen, H. B.; Huan, W.; Li, J. Q.; Zhai, M. L. Epoxy-POSS/silicone rubber nanocomposites with excellent thermal stability and radiation resistance. *Chinese Chem. Lett.* **2022**, *33*, 3534–3538.
[21] Zhang, Y. B.; Yan, H. X.; Xu, P. L.; Guo, L. L.; Yang, K. M.; Liu, R.; Feng, W. X. A novel POSS-containing polyimide: Synthesis and its composite coating with graphene-like MoS_2 for outstanding tribological performance. *Prog. Org. Coat.* **2021**, *151*, 106013.
[22] Cherkashina, N. I.; Pavlenko, V. I.; Noskov, A.V.; Shkaplerov, A. N.; Kuritsyn, A. A.; Popova, E. V.; Zaitsev, S. V.; Kuprieva, O. V.; Kashibadze, N. V. Synthesis of PI/POSS nanocomposite films based on track nuclear membranes and assessment of their resistance to oxygen plasma flow. *Polymer* **2021**, *212*, 123192.
[23] Zhang, S. M.; Chen, W.; Hao, W.; Li, D.; Zhang, C. C.; Yu, F.; Chen, Y. A composite gel polymer electrolyte by incorporating modified POSS endowing inorganic-rich SEI formation and stable cycle life for lithium metal batteries, *Chem. Eng. J.* **2024**, *484*, 149499.
[24] Yao, M. Z.; Liu, Y.; Qin, C. N.; Meng, X. J.; Cheng, B. X.; Zhao, H.; Wang, S. F.; Huang, Z. Q. Facile fabrication of hydrophobic cellulose-based organic/inorganic nanomaterial modified with POSS by plasma treatment. *Carbohyd. Polym.* **2021**, *253*, 117193.
[25] Deng, S. L.; Xu, X. F.; Fan, C. L.; He, Q. L.; Wang, Y. Q. Constructing pod-like $ZnFe_2O_4$@SiO_2@C composite fibers network structure to enhance impedance matching for efficient microwave absorption. *Colloid. Surface. A* **2025**, *727*, 138430.
[26] Jin, Y. Z.; Fan, C. M.; Zhang, Q. L.; He, Q. C.; Wang, Y. Q. Constructing core–shell SiC@C nanofiber network structures to enhance conductive loss for efficient microwave absorption. *Inorg. Chem. Front.* **2025**, *12*, 7590–7602.
[27] Hou, T. Q.; Liu, X.; Ren, J. W.; Xu, X. Z.; Lan, D.; Zhang, S. Y.; Guo, H.; Wu, G. R.; Jia, Z. R.; Wu, G. L.; Mesoporous hollow silica with controlled particle size for optimizing dielectric properties and coefficient of thermal expansion of polyimide packaging materials. *J. Mater. Sci. Technol.* **2025**, *235*, 122–132.
[28] Zhang, W. L.; Xu, S.; Li, X.; Yin, Y. H.; Sun, C. L.; Yu, Z. L.; Zhao, C.; Lan, D.; Jia, Z. R.; Wu, G. L.; Xu, X. Z. Mesoporous Hollow Carbon Spheres/Nanofibers Anchored with Conductive Bimetallic for Efficient Microwave Absorption. *Rare Met.* **2025**, doi: 10.1002/rar2.70051.
[29] Dong, J.; Li, L. Q.; Qiu, P.; Pan, Y. P.; Niu, Y. J.; Sun, L.; Pan, Z. Z.; Liu, Y. Q.; Tan, L.; Xu, X. W.; Xu, C.; Luo, G. F.; Wang, Q.; Wang, H. Scalable Polyimide-Organosilicate Hybrid Films for High-Temperature Capacitive Energy Storage. *Adv. Mater.* **2023**, *35*, 2211487.
[30] Qiao, G. Y.; Wang, X. X.; Li, X.; Li, J.; Geng, K. Y.; Jin, E. Q.; Xu, J. J.; Yu, J. H. Unlocking synthesis of polyhedral oligomeric silsesquioxane-based three-dimensional polycubane covalent organic frameworks, *J. Am. Chem. Soc.* **2024**, *146*, 3373–3382.
[31] Qian, M.; Murray, V. J.; Wei, W.; Marshall, C. B.; Minton, K. T. Resistance of POSS polyimide blends to hyperthermal atomic oxygen attack. *ACS Appl. Mater. Interfaces* **2016**, *8*, 33982–33992.
[32] Minton, T. K.; Wright, M. E.; Tomczak, S. J.; Marquez, S. A.; Shen, L. H.; Brunsvold, A. L.; Cooper, R.; Zhang, J. M.; Vij, V.; Guenthner, A. J.; Petteys, B. J. Atomic oxygen effects on POSS polyimides in low earth orbit. *ACS Appl. Mater. Interfaces* **2012**, *4*, 492–502.
[33] Wu, H.; Zhang, Y.; Guo, Y. D.; Qi, H. R.; An, Y. C.; Jia, Y. J.; Tan, Y. Y.; Liu, J. G.; Wu, B. H. Preparation and properties of intrinsically atomic-oxygen resistant polyimide films containing polyhedral oligomeric silsesquioxane (POSS) in the side chains. *Polymers* **2020**, *12*, 2865.
[34] He, Y. J.; Suliga, A.; Brinkmeyer, A.; Schenk, M.; Hamerton, I. Effect of atomic oxygen exposure on polybenzoxazine/POSS nanocomposites for space applications. *Compos. Part. A-Appl. S.* **2024**, *177*, 107898.
[35] Nam, K. H.; Jin, J.; Lee, D. H.; Hanc, H.; Goha, M.; Yua, J.; Kua, B. C.; You, N.H. Towards solution-processable, thermally robust, transparent polyimidechain-end tethered organosilicate nanohybrids. *Compos. Part. B-Eng.* **2019**, *163*, 290–296.
[36] Rethinasabapathy, M.; Hwang, S. K.; Kang, S. M.; Roh, C.; Huh, Y.S. Amino-functionalized POSS nanocage-intercalated titanium carbide (Ti_3C_2Tx) MXene stacks for efficient cesium and strontium radionuclide sequestration. *J. Hazard. Mater.* **2021**, *418*, 126315, doi: 10.1016/j.jhazmat.2021.126315.
[37] Zhang, P. P.; Zhao, J. P.; Zhang, K.; Bai, R.; Wang, Y. M.; Hua, C. X.; Wu, Y. Y.; Liu, X. X.; Xu, H. B.; Li, Y. Fluorographene/polyimide composite films: mechanical, electrical, hydrophobic, thermal and low dielectric properties. *Compos. Part A-Appl. S.* **2016**, *84*, 428–434.
[38] Cheng, X.; Wang, C. X. ; Chen, S. ; Zhang, L. Y.; Liu, Z. L.; Zhang, W. H. Preparation the high mechanical performance of MoS_2@PDA modified polyimide film for enhanced electrical insulation. *Polymers* **2024**, *16*, 546.
[39] Wang, C. X.; Liu, Y.; Jia, Z. R.; Zhao, W. R.; Wu, G. L. Multicomponent Nanoparticles Synergistic One-Dimensional Nanofibers as Heterostructure Absorbers for Tunable and Efficient Microwave Absorption. *Nano-Micro Lett.* **2023**, *15*, 2311-6706.
[40] Pan, Y. L.; Yu, K. L.; Lan, Di; Zhang, Z. L.; Chen, Z. S. Multiple Selenide Modified Carbon Fibers to Construct Heterogeneous Interfaces for Electromagnetic Wave Absorption. *Carbon* **2025**, *245*, 120824.
[41] Zhang, Q. L.; Lan, D.; Deng, S. L.; Gu, J. W.; Wang, Y. Q.; Ren, J. W.; Wu, G. L.; Jia, Z. R. Constructing multiple heterogeneous interfaces in one-dimensional carbon fiber materials for superior electromagnetic wave absorption. *Carbon* **2024**, *226*, 119233.
[42] Han, Z. D.; Zhang, W. Y.; Song, X. N.; Vahabi, H. R.; Pan, Y. T.; Zhang, W. C.; Yang, R. J. Fast char formation induced by POSS confining Co-MOF hollow prisms in epoxy composites with mitigated heat and smoke hazards. *Chem. Eng. J.* **2023**, *474*, 145682.
[43] Dong, H.; Dong, J.; Li, X. T.; Zhao, X.; Xu, Q. S.; Zhang, J. L.; Zhang, Q. H. Preparation of high-temperature resistant polyimide fibers by introducing the p- phenylenediamine into kapton-type polyimide. *ACS Appl. Polym. Mater.* **2024**, *6*, 2371–2380.
[44] Du, X.; Yan, F. F.; Cheng, M. T.; Li, H. Y.; Peng, C.; Liu, Y. L.; Liu, Dong; Lan, D.; Wu, G. L.; Jia, Z. R. Dual-Functional Core-Shell Composites: Integrated Microwave Absorption and Thermal Management Properties. *Int. J. Miner. Metall. Mater.* **2025**, doi: 10.1007/s12613-025-3317-1.
[45] Jia, Z. C.; Wang, H. Y.; Yu, P.; He, H. F.; Huang, Q. R.; Hong, W.; Liu, C.; Shi, Y. J.; Wang, J.; Xin, Y. M.; Jia, X. M.; Ma, J. J.; Yu, B. Soft-rigid construction of mechanically robust, thermally stable, and self-healing polyimine networks with strongly recyclable adhesion. *Small* **2024**, *20*, 2406821.
[47] Xiao, S. D.; Akinyi, C.; Longun, J.; Iroh, J. O. Polyimide Copolymers and Nanocomposites: A Review of the Synergistic Effects of the Constituents on the Fire-Retardancy Behavior. *Energies* **2022**, *15*, 4014.
[48] Ye, X. M.; Feng, Y.; Tian, P. P.; Li, Z. M.; Li, Y. C.; Wang, W. S.; Li, J.; Qiao, L.; Wang, K.; Zhang, W. C.; Pan, Y. T.; Yang, R. J. Engineering two nitrogen-containing polyhedral oligomeric silsesquioxanes (N-POSSs) to enhance the fire safety of epoxy resin endowed with superior thermal stability. *Polym. Degrad. Stabil.* **2022**, *200*, 109946.
[49] Sun, Y.; Zhang, Y.; Shi, H. Y.; Wang, S. J.; Liu, J. L.; Luo, Y.; Zhang, C.; Zhang, K.; Li, S. X.; Fan, W. Hierarchically engineered flame-retardant triboelectric yarn exhibiting robust mechanical performance and humidity-boosted electrical output for firefighting applications. Adv. Mater. **2025**, *12*, e07673.
[50] Peng, J. J.; Zhang, G. J.; Duan, Y. R.; Wang, H. B.; Zhang, Y. Green crosslinking strategy for ethylene-vinyl acetate rubber composites with NH_2-POSS as a crosslinking agent and reinforcing nanofiller. *Compos. Sci. Technol.* **2024**, *257*, 110808.
[51] Wang, H. M.; Li, L.; Zhang, T.; Zheng, S. X. Organic-inorganic

polyureas with benzyl hindered urea bonds and POSS cages in the main chains: Synthesis, shape memory and reprocessing properties. *Eur. Polym. J.* **2024**, *202*, 112652.
[52] Guo, Y. Q.; Zhang, L.; Ruan, K. P.; Mu, Y.; He, M. K.; Gu, J. W.; Enhancing hydrolysis resistance and thermal conductivity of aluminum nitride/polysiloxane composites via block copolymer-modification. *Polymer* **2025**, *323*, 128189.
[53] Zhang, Y. Y.; Hu, T.; Hu, R. B.; Jiang, S. H.; Zhang, C. M.; Hou, H. Q. Thermal, mechanical and dielectric properties of polyimide composite films by in-situ reduction of fluorinated graphene. *Molecules* **2022**, *27*, 8896.
[54] Liu, J. L.; Wu, Z.; Tao, Y.; Sun, Y.; Shi, H. Y.; Liu, Y.; Song, H. L.; Zhang, C.; Wang, S. J.; Fan, W. Green-orange bi-color switchable mechanoluminescent fiber of okra-like structure for visual signaling. Adv. Mater. **2025**, https://doi.org/10.1002/adma. 202515254.
[55] Hu, T.; Lan, D.; Wang, J.; Zhong, X. Z.; Bu, G. X.; Yin, P. F. Construction of $NiCo_2O_4$/$NiCoO_2$ co-embedded porous bio-carbon with rich heterogeneous interfaces for excellent bacteriostatic microwave radiation protection. *Carbon* **2025**, *232*, 119798.
[56] Wang, C. X.; Jia, Z. R.; He, S. Q.; Zhou, J. X.; Zhang, S.; Tian, M. L.; Wang, B. B.; Wu, G. L. Metal-organic Framework-derived nanocubes as absorbers for electromagnetic wave attenuation. *J. Mater. Sci. Technol.* **2022**, *108*, 236-243.
[57] Zhou, J. X.; Huang, X. M.; Lan, D.; Jia, Z. R.; Wu, G. L. Multi-interface polarization engineering constructs one-dimensional carbon nanocages heterostructures for efficient electromagnetic wave absorption. *Carbon* **2026**, *248*, 121143.
[58] Peng, Z. Y.; Ye, A.; Zhang, L.; Li, X.; Li, X. L.; Lian, C.; Li, C. Z. Micro-crosslinked polyimide nanocomposites with low dielectric constant and low dielectric loss for microwave antenna with molecular dynamics. *Compos. Commun.* **2024**, *46*, 101804.
[59] Wei, Y. H.; Yang, L. H.; Wang, C.; Zhu, Z. Y.; Dai, Y. C.; Qin, H. M.; Xiong, C. X. Enhanced high-temperature capacitive energy storage in polyetherimide dielectrics through dense crosslinked network structures. *Chem. Eng. J.* **2025**, *507*, 160793.
[60] Ren, X. Y.; Jia, Z. R.; Gao, Z. G.; Zhang, S. Y.; Zhang, Yu.; Lan, Di.; Wu, G. L. Synergistic Band and Multiscale Hybrid Engineering in Polycrystalline TiO_2 for Enhanced Spatial Charge Polarization Relaxation. *Adv. Funct. Mater.* **2025**, doi: 10.1002/adfm.202524264.
[61] Yang, K. R.; Dai, J. Y.; Zhao, W. W.; Wang, S. P.; Liu, X. Q. Bio-based epoxy resin demonstrating high breakdown strength and low dielectric loss via intrinsic molecular charge traps construction. *Compos. Part. B-Eng.* **2024**, *284*, 111728.
[62] Li, X.; He, T. J.; Yin, Q.; Qin, Y. T.; Sun, S. Y.; Yang, J.; Wang, P.; Fan, K.; Liu, X. Y. Fluorinated Al_2O_3/siloxane modified PI films towards vastly enhanced corona resistance performance. *Compos. Part. A-Appl. S.* **2023**, *172*, 107613.
[63] Shi, M. J.; Jia, Z. R.; Lan, D.; Gao, Z. G.; Zhang, S. Y.; Wu, G. L. Type-II Heterojunction Regulated BIEF towards Nitride/chalcogenide semiconductors for Multi-Polarization Relaxation. *Adv. Funct. Mater.* **2025**, doi: 10.1002/adfm.202528665.

Electronic Supplementary Material

Polyhedral oligomeric silsesquioxane (POSS) constructed stable cross-linking network in polyimide for enhanced flame retardant, mechanical and corona resistance properties

Xian Cheng[1,§], Chenxi Wang[1,§] ✉, Di Lan[2], Zihao Tang[1], Shuo Chen[1], Wenhao Zhang[1], Xinfeng Zhou[3], Leyuan Zhang[1], and Guanglei Wu[4]✉

[1] *School of Electrical and Information Engineering, Zhengzhou University, Zhengzhou 450001, China*
[2] *School of Automotive Materials, Hubei University of Automotive Technology, Shiyan 442002, China*
[3]*Beijing Key Laboratory of Advanced Functional Polymer Composites, Beijing University of Chemical Technology, Beijing 100029, China*
[4]*College of Materials Science and Engineering, Qingdao University, Qingdao 266071, China*
[§]*Xian Cheng and Chenxi Wang contributed equally to this work.*

✉Address correspondence to Chenxi Wang, chengxian@zzu.edu.cn; Guanglei Wu, wuguanglei@mail.xjtu.edu.cn, wuguanglei@qdu.edu.cn

Supporting information to https://doi.org/10.26599/NR.2026.94908433

Address correspondence to Xian. Cheng, chengxian@zzu.edu.cn; Chenxi Wang, m15897696905@163.com; Guanglei Wu, wuguanglei@qdu.edu.cn

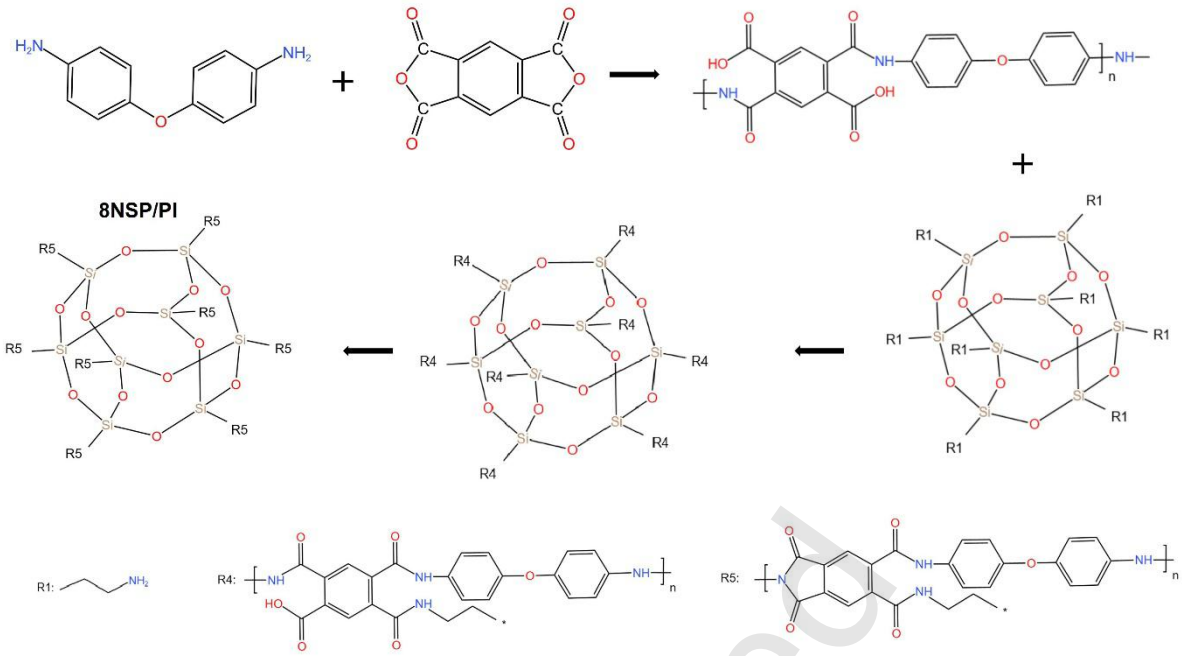

Figure S1 The synthetic reaction equation schematic diagram of 8NSP/PI.

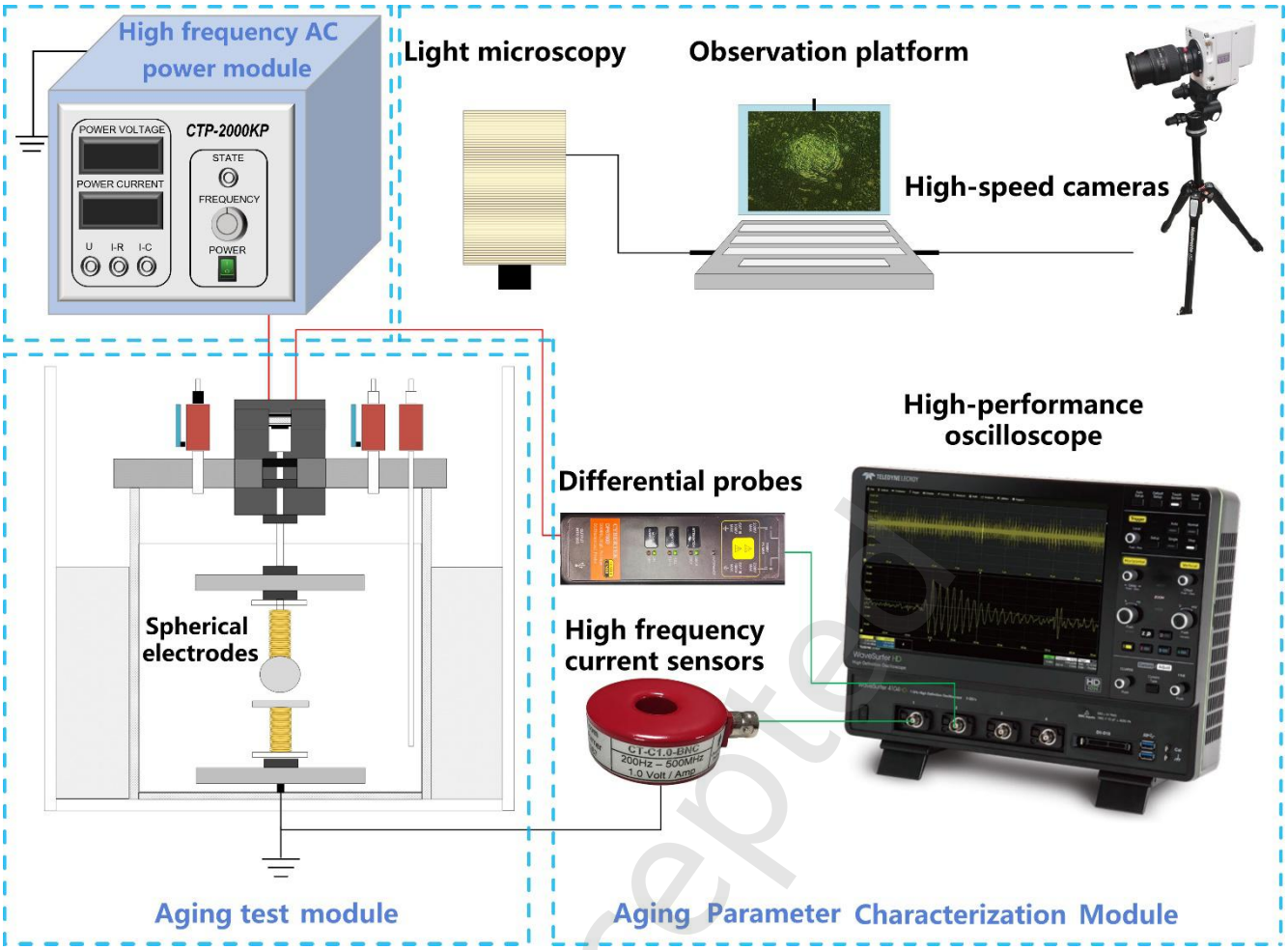

Figure S2 Breakdown and corona resistance of PI and other composite films test systems.

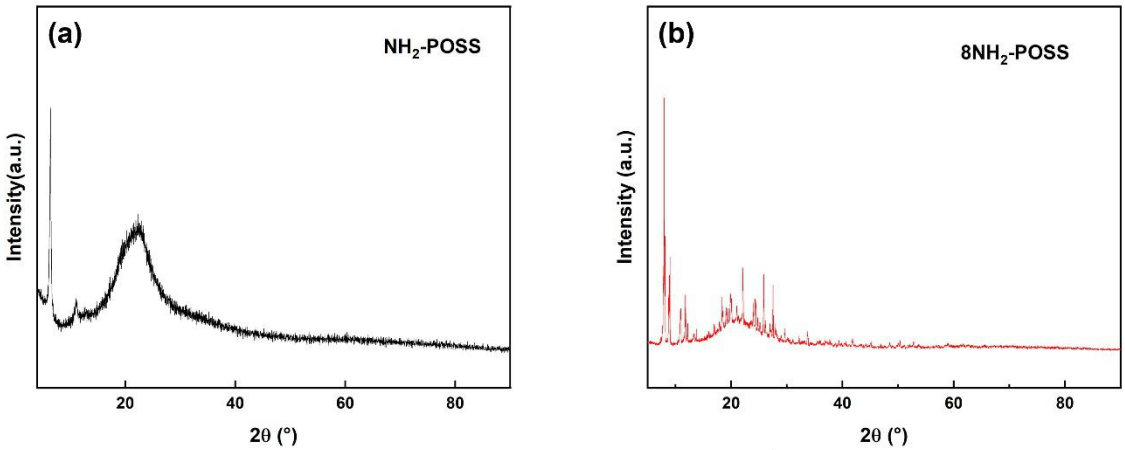

Figure S3 The XRD spectrum of NH_2-POSS (a) and $8NH_2$-POSS (b).

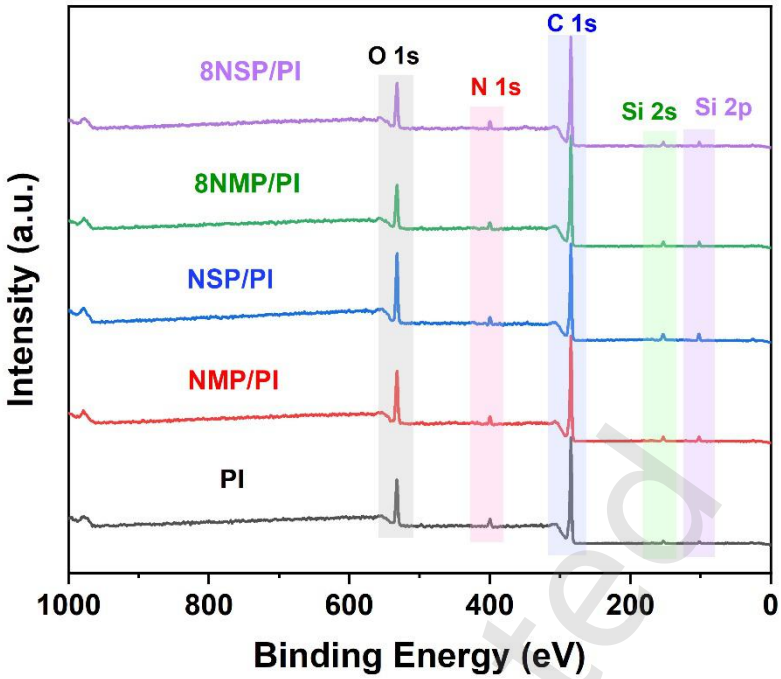

Figure S4 XPS full spectrum of PI, NMP/PI, NSP/PI, 8NMP/PI and 8NSP/PI.

Figure S5 UL-94 digital images of PI.

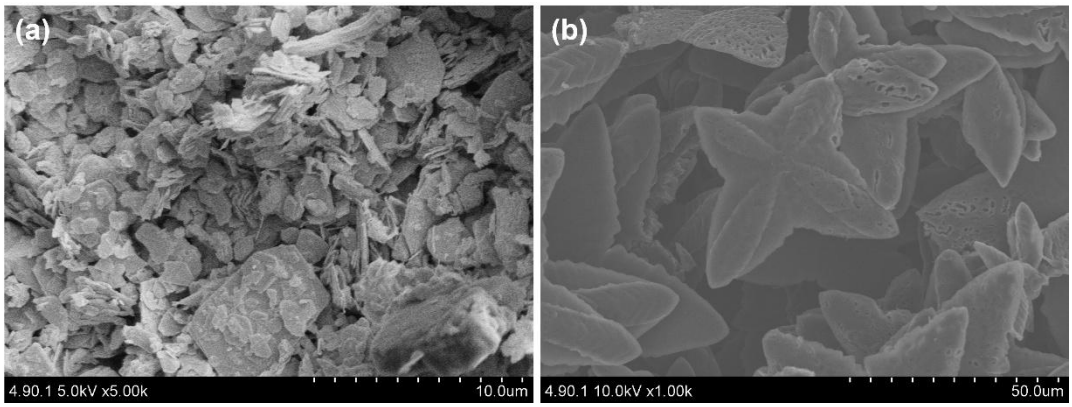

Figure S6 The SEM of images NH_2-POSS (a) and $8NH_2$-POSS (b).

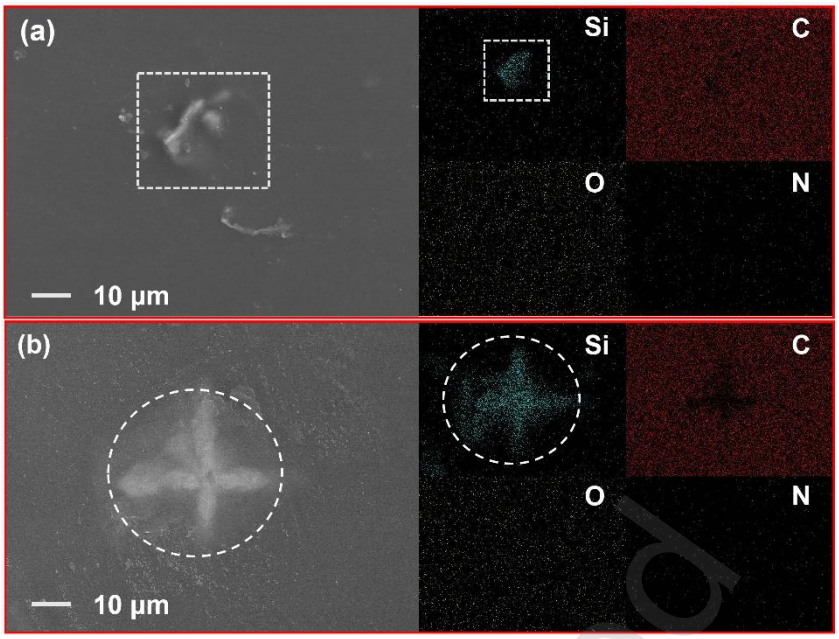

Figure S7 The SEM and energy dispersive spectroscopy (EDS) mapping images of the 8NMP/PI (a) and 8NSP/PI (b).

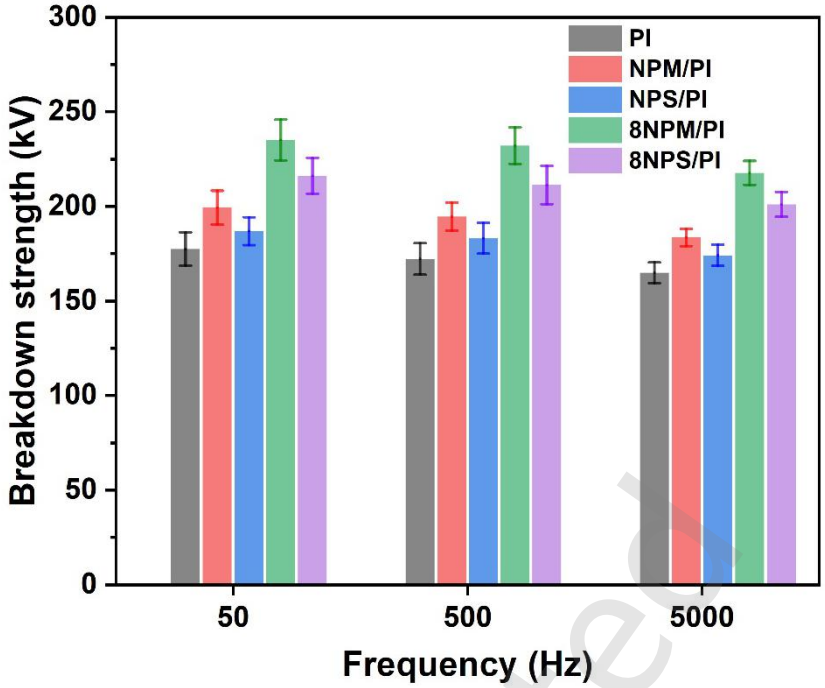

Figure S8 The average breakdown field strength and error bars of PI, NMP/PI, NSP/PI, 8NMP/PI and 8NSP/PI at 50, 500 and 5000 Hz.

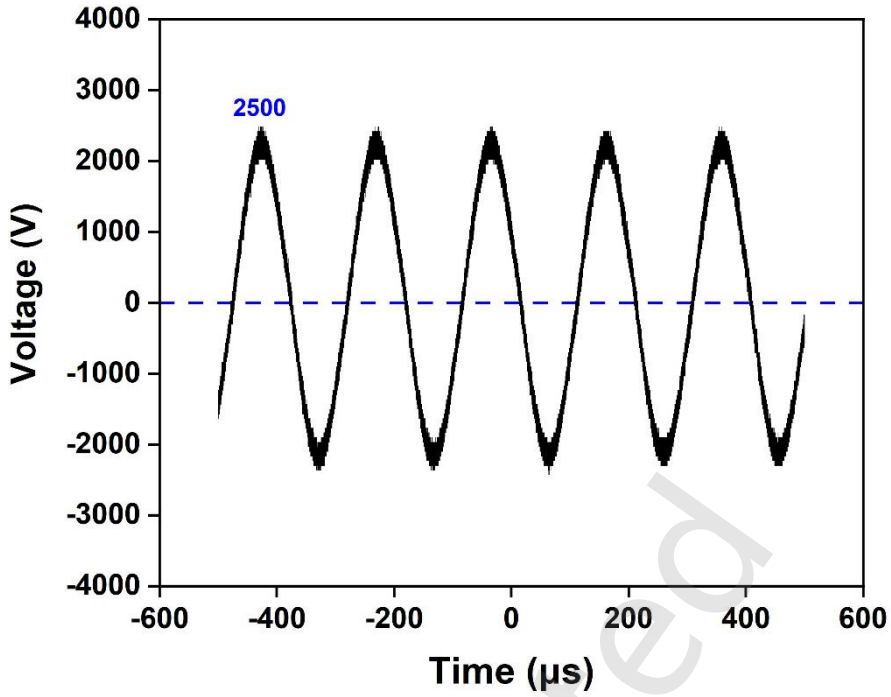

Fig. S9. The accelerated aging voltage waveform at 2.5 kV-5kHz.

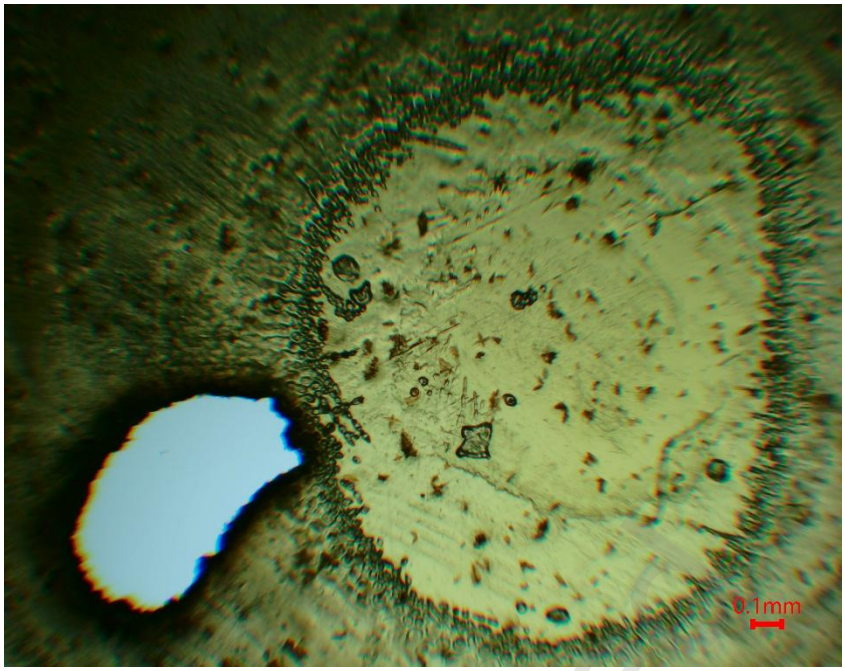

Fig. S10. The optical micrograph of the central breakdown region of the 8NMP/PI film.